Journal of Applied Electrochemistry (2006) 36:1381–1389
DOI 10.1007/s10800-006-9220-1


# The influence of bubble shape and the thickness of the wetting film on the incremental electrical resistance caused by the presence of a single bubble in Hall-Héroult cells

A.L. PERRON, L.I. KISS* and S. PONCSÁK
*Département des sciences appliquées, Université du Québec à Chicoutimi, Quebec, Canada G7H 2B1*
*(*author for correspondence, tel.: + 1-418-545-5011, fax: + 1-418-545-5012, e-mail: lkiss@uqac.ca)*

Received 21 February 2006; accepted in revised form 15 August 2006

*Key words:* alumina reduction cell, bubble shape, gas bubbles, interelectrode resistance

**Abstract**

Bubbles play an important role in the transport phenomena existing in an electrolysis cell. They increase the total ohmic resistance of the electrolyte but their contribution is still not well quantified. During their movement under the anode, the bubbles are separated from the solid by the so-called wetting film, that is by a thin liquid layer. In order to develop a mathematical model to compute the increment of the electrical resistance of the electrolyte due to the presence of several bubbles under the anode, the effects of the bubble shape and the thickness of the wetting film for a single bubble must be quantified *a priori*. In this first paper, these effects are computed using the finite element method (FEM). The results have shown that the influence of the bubble shape and that of the wetting film is small, about 5% and 2%, respectively.

**List of symbols**

| | |
|---|---|
| $A_a$ | anode area ($m^2$) |
| $A_p$ | projected area ($m^2$) |
| $A^*$ | cross-section of an electrical current tube ($m^2$) |
| $b$ | bubble front width (m) |
| $d$ | bubble diameter (m) |
| $d_{eq}$ | equivalent diameter (m) |
| $\vec{E}$ | electrical field (V/m) |
| $g$ | gravitational acceleration (m $s^{-2}$) |
| $h$ | bubble height (m) |
| $i$ | local current density (A $m^{-2}$) |
| $\vec{i}$ | current density vector (A $m^{-2}$) |
| $I$ | current (A) |
| $L_C$ | length of the elongated bubble (m) |
| $r$ | geometrical ratio for large bubbles |
| $R_0$ | electrical resistance of the bubble-free electrolyte ($\Omega$) |
| $R_T$ | total electrical resistance of the electrolyte with bubbles present ($\Omega$) |
| $u_T$ | bubble terminal velocity (m $s^{-1}$) |
| $V$ | voltage (V) |
| $V^*$ | bubble volume ($m^3$) |

**Greek symbols**

| | |
|---|---|
| $\kappa$ | electrical conductivity ($\Omega^{-1}$ $m^{-1}$) |
| $\Theta$ | covering factor |
| $\rho$ | density (kg $m^3$) |
| $\sigma$ | surface tension (N m) |
| $\upsilon$ | kinematic viscosity ($m^2$ $s^{-1}$) |

**Subscripts**

| | |
|---|---|
| 1 | anode |
| 2 | electrolyte |
| A | upper limit of the computational domain (within the anode) |
| B | cathode surface (bath-molten aluminium interface) |
| l | liquid phase |
| $n$ | index of an element |
| $n$ | normal component |
| $N$ | number of element |
| $t$ | tangential component |

**Superscript**

| | |
|---|---|
| * | electrical current tube |

## 1. Introduction

In the Hall-Héroult process, liquid aluminium is produced by the electrolytic reduction of alumina ($Al_2O_3$) dissolved in an electrolyte of essentially cryolite ($Na_3AlF_6$) at about 960 °C [1]. In a typical cell, the anode and the cathode are arranged horizontally. The primary cell reaction is

$$2/3Al_2O_3 + C = 4/3Al + CO_2. \quad (1)$$

The current which passes through the cell is the in order of 100 kA. The consumption of the anode is about 1.5 cm per day. The prebaked anodes have to be replaced usually after 22–26 days. The liquid aluminium is deposited at the cathode and bubbles, principally composed of $CO_2$, are generated under the anode surface. When the bubbles reach a critical size which depends principally on the anode local slope, the electrolyte velocity field as well as the retention forces, they start to move, escape from the anode sides. It is believed that when a bubble reaches a certain velocity, there is a dynamical formation of a thin wetting film separating the bubble and the anode surface. The formation of the film has been observed experimentally in an air–water–plexiglas system [2]. The direct observation in a real industrial cell is impossible, owing to its small thickness and the opacity as well as the corrosivity of the cryolite. The presence of the bubbles (stationary and moving) under the anode contributes to increase the ohmic resistance of the electrolyte. According to Haupin [3], the extra ohmic drop is in the range of 0.15–0.35 V.

Since the pioneering work of Dernedde and Cambridge [4] about three decades ago, a lot of research has been devoted to the role of bubbles in the Hall-Héroult process. The contribution of the bubbles to the induced bath flow, to the cell thermal balance as well as to the total resistance of the electrolyte is still not well understood. The knowledge of the contribution of the bubbles to the overvoltage of the cell is an important parameter to estimate the value of the anode–cathode distance ACD under normal electrolysis conditions. In order to elaborate a mathematical model to compute the total resistance of the electrolyte, the effect of bubble shape and the thickness of the wetting film must be quantified *a priori*. The term total resistance $R_T$ refers to the electrical resistance of the electrolyte in the entire interelectrode spacing when bubbles are present. In this work, the increase of the electrical resistance caused by the presence of the bubbles is expressed in a relative manner by dividing the total electrical resistance $R_T$ by the resistance $R_0$ of the bubble-free electrolyte.

Hyde and Welch [5] studied the influence of accumulated gas under the anode, the ACD and the bubble shape on the bubble resistance. The bubbles were simulated by ceramic objects of known volume and shape. The tested shapes were discs and spheres. The objects were inserted in a laboratory electrolysis cell producing lead. The electrical resistance of the electrolyte with and without bubbles was obtained by measuring the voltage drop of the cell with a high sampling rate when the current was suddenly stopped. This procedure allowed the separation of the voltage components of the laboratory cell. The results showed that the resistance increase caused by the presence of the bubbles (solid objects) primarily depends on the bubble volume, and it increases linearly with the accumulated gas (ceramic objects). The effect of bubble shape on the resistance increase has been found to be small for the same amount of accumulated gas. Aaberg et al. [6] investigated the characteristics of the bubble layer under the anode in a small scale electrolysis cell producing aluminum. The diameter of the carbon anode was less than 10 cm. By measuring simultaneously the volume of the accumulated gas and the electrical resistance of the electrolyte, they deduced the covering factor and the thickness of the bubble layer. The expressions to compute the latter quantities were based on the work of Hyde and Welch [5] which considered the bubbles as equivalent cylinders with a diameter equal to the depth of the bubble layer. The volume of gas was obtained by measuring the rise of the electrolyte level, as done by Solheim and Thonstad [7]. As pointed out by Quian et al. [8], this measurement method may introduce an error since the bubbles outside the interpolar region are included in the total accumulated gas. Nevertheless the typical covering factor measured was about 45%. The thickness of the bubble layer varied from 4 to 6 mm. The average value of the accumulated gas under the anode was 0.445 $cm^3/cm^2$. Haupin [3] measured the voltage gradient in the interpolar space in an industrial reduction cell. He measured a thickness of 5 mm for the bubble layer. He found that occasionally, there were contacts between the probe and gas bubbles as far as 2 cm from the anode surface.

Zoric and Solheim [9] were the first to include the effect of the perturbation of the electrical field in the entire ACD caused by the presence of bubbles in their calculation of the electrical resistance. They studied the anodic and cathodic current distribution perturbed by the presence of bubbles. The bubbles were represented by large discrete slabs 5 mm thick. They also modeled large bubbles with a thicker (deeper) front (1–1.5 cm). The length of the bubble varied from 24 to 75 mm. In all cases, the anodic current density reached local maxima close to the bubble. The local minima of the cathodic current density were not significantly influenced by the bubble position because of the long distance between the bubble and the cathode. They also presented some correlations for the incremental voltage drop applicable in certain conditions.

The aim of this work is to compute the influence of the bubble shape and the thickness of the wetting film on the relative resistance caused by the presence of single bubbles under the anode.

## 2. The mathematical model

To calculate the relative resistance $R_T/R_0$ induced by the presence of the bubbles underneath the anode, the Laplace equation

$$\nabla^2 V = 0 \tag{2}$$

is solved within the domain with the cross-section shown in Figure 1. In order to analyze the influence of all the different bubble shapes used in the present paper, the

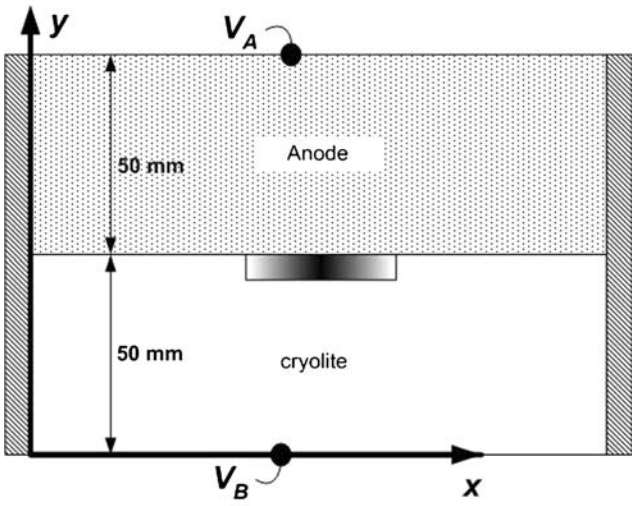


*Fig. 1.* Cross-section of the 3D model.

domain is three-dimensional. The computational domain is multiply connected: there is an external boundary and an internal one around the bubble. The conservation of the electric charge requires that the normal component of the current density vector is continuous at the anode–electrolyte interface:

$$i_{1n} = i_{2n}. \tag{3}$$

Using the differential form of the Ohm's law ( $\vec{i} = \kappa\vec{E}$) this becomes

$$\frac{E_{1n}}{E_{2n}} = \frac{\kappa_2}{\kappa_1}. \tag{4}$$

The other part of the coupling conditions comes from the equality of the electric field strength on the two sides of the interface. Thus the tangential components of $\vec{E}$ are equal on the two sides:

$$E_{1t} = E_{2t}. \tag{5}$$

The anode–cathode distance ACD is assumed to be 5 cm. The distance between the upper equipotential plane (within the anode) and the cathode surface is fixed at 10 cm. The resistivity of the electrolyte and the anode were taken to be 0.5 Ωcm and 0.005 Ωcm, respectively [9]. The Laplace equation is an elliptic PDE type therefore the boundary conditions on the complete contour enclosing the geometry must be specified to obtain a solution. The boundary conditions are simply those of the first kind

$$V(y = 0) = V_B, \tag{6}$$

$$V(y = L) = V_A. \tag{7}$$

Furthermore, the vertical limits on the left and right side of the domain and the bubble interface were considered insulated

$$\frac{\partial V}{\partial n} = 0. \tag{8}$$

where $n$ is the normal to the domain limits or to the bubble interface. The boundary-value problem was solved using the finite element method. To study the effect of bubble shape, a mesh with about 60,000–100,000 tetrahedral elements was generally used. The characteristic length of the elements was less than 3 mm. A mesh control was used to compute the effect of the thin wetting film on the relative resistance. The thickness of the elements in the $y$ direction within the wetting film was less than 0.1 mm.

Several calculations of the relative resistance were also carried out with an equipotential electroactive area of the anode, similarly as done by Vogt and Kleinschrodt [10]. In other words, the distance between the upper equipotential plane and the cathode surface was reduced to 5 cm. The relative resistances calculated within the two different computational domains were very similar. This may be explained by the high ratio of resistivity of the electrolyte on the anode. In this situation, there were also current density maxima along the bubble contour.

The total current provoked by a constant voltage (boundary condition of first kind) through the domain where a bubble is present is given by

$$I_T = \int_A i dA = \sum_{n=1}^{N} i_n dA_n \tag{9}$$

where $A$ is the total cathode surface, $N$ is the number of elements on the cathode surface and, $i_n$ and $dA_n$ are the local current density and the area of the $n$th cathode element, respectively. The relative bubble resistance is evidently independent of the order or type of the boundary conditions. Then

$$\frac{R_T}{R_0} = \left.\frac{V_T}{V_0}\right|_{I=\text{const}} = \left.\frac{I_0}{I_T}\right|_{V=\text{const}} \tag{10}$$

where $R_T$ and $R_0$ are the electrical resistance of the total electrolyte and the bubble-free electrolyte, respectively. It is clear that this model neglects some phenomena. The model computes only the primary current distribution. The addition of the anodic activation overvoltage would tend to homogenize the current distribution close to the bubble. It assumes a non-deformable cathode surface and the bubble shapes are also well defined. It neglects the effect of convection on the transport of sodium charge carriers. In other words, in the solution domain the conductivity of the bubble-free electrolyte is assumed to be homogeneous and isotropic. In this work, the results are presented in a relative form which emphasizes the role of the bubble on the total electrical resistance.

## 3. Results and discussion

In this section, the results concerning the difference of the relative bubble resistance caused by four different

bubble shapes of the same volume are presented first. In the second part, the effect of the thickness of the wetting film on the electrical resistance is discussed. The liquid film is located between the anode and the moving bubble. It separates the anode surface and the moving bubbles.

### 3.1. *The influence of bubble shape*

The dynamic shape of a bubble depends of the forces which act on it. In a gravity driven flow, Kiss et al. [2] and Perron et al. [11] have shown that there may exist two main classes of bubbles moving under a solid surface: the "creeping bubble" and the "bubble on the wetting film". In the former, the terminal velocity is controlled by the surface tension, the buoyancy and the viscous forces. However, in an industrial cell, the buoyancy acting on the bubble is not the only driving force, i.e. there is a drag force generated by the flow around the bubble. The distance traveled by the creeping bubble in a real cell is very small. Consequently in this work, the bubble shape observed in the creeping regime is not studied. For the bubble on the wetting film, the inertia may play the dominant role in controlling the movement. However, a recent study [12] showed that the viscous and surface tension forces play also a non-negligible role at both low bubble volumes and low inclination angles of the solid surface.

The bubble shapes studied in this paper are based on shapes observed in the above mentioned study [12], on other visual observations and on the well-known work of Fortin et al. [13]. All the bubble shapes reported here including the Fortin's shape are observed in an air–water two-phase flow system. A recent study [14] has shown that the bubble motion under an inclined surface may be described by three independent dimensionless parameters such as the Bond and Morton numbers, the inclination angle and by one dependent parameter, the Reynolds number. If the effects of the physical properties of the dispersed phase are neglected, the Morton, Bond and Reynolds numbers are expressed as

$$Mo = \frac{g\upsilon_l^4\rho_l^3}{\sigma^3} \quad Bo = \frac{\rho_l d^2 g}{\sigma} \quad Re = \frac{u_T d}{\upsilon_l} \tag{11}$$

where $\rho_l$ is the liquid density, $\upsilon_l$ is the liquid kinematic viscosity, $g$ is the gravitational acceleration, $\sigma$ is the surface tension, $u_T$ is the bubble terminal velocity and $d$ is the bubble equivalent diameter defined by $d = (6V^*/\pi)^{1/3}$, where $V^*$ is the bubble volume. Thus, the Morton number depends strictly on the physical properties of the working liquid. The values of the Morton number for the water at 20 °C and cryolite under normal operation conditions are $2.59 \times 10^{-11}$ and $9.46 \times 10^{-11}$, respectively. Therefore, one assumes that the observed bubble shapes in water may exist in the cryolite under normal operation conditions.

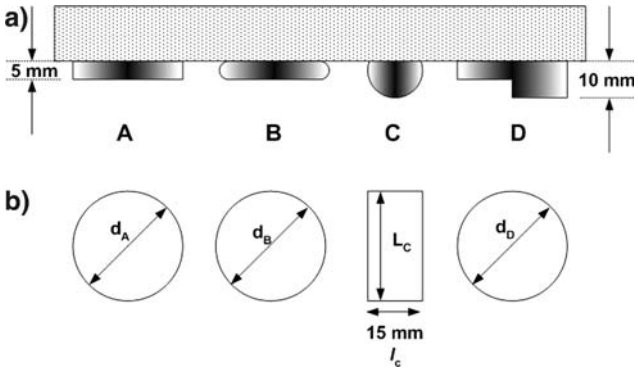


*Fig. 2.* Bubble shapes used in this work: (a) lateral view, (b) top view.

The four basic bubble shapes are presented in Figure 2. The volume of the bubble A is given by

$$V_A^* = \frac{\pi d_A^2}{4} h_A \tag{12}$$

where $h_A$ is the depth of the bubble and its value is 0.5 cm. The bubble shape A is not an observed one. It is used only as a simplification to ease computational work, since its geometry is simple. Henceforth, the bubble shape A is called *circular disc*. Although the shape B has been observed experimentally in water at both low bubble volumes and low inclination angles, the principal reason to study this shape is the fact that the bubble simulator developed by Kiss et al. [15–17] uses this bubble shape. The volume of the bubble B is

$$V_B^* = \pi h\left(\frac{d_B^2}{4} - \frac{h_B d_B}{4} + \frac{h_B^2}{6}\right). \tag{13}$$

The depth of this bubble is also 0.5 cm. From now, the bubble shape B is called *rounded disc*. For larger bubble volumes and/or for higher bubble velocities, the bubble becomes more deformable and the depth of the bubble may be greater than 0.5 cm. This deformation is caused by a perturbation moving with the same velocity as the bubble and it is called a hydraulic jump. The

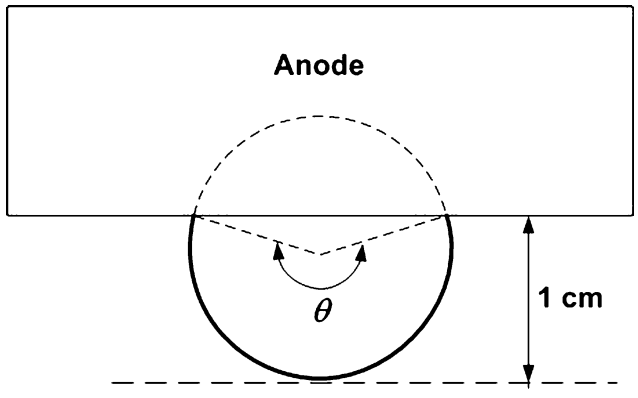


*Fig. 3.* Definition of θ used to describe the bubble shape C.

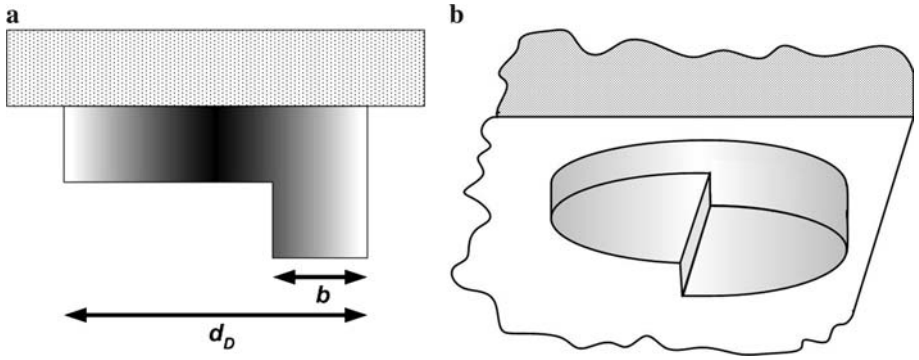


*Fig. 4.* Bubble shape D (Fortin shape): (a) lateral view, (b) bottom view.

phenomenon has been first observed (indirectly) by Haupin [3]. The shapes C and D represent this situation. The former has been observed by Perron et al. [12] for bubble volumes ranging from about 5 to 15 $cm^3$. The length of the bubble C in the direction parallel to the movement, $l_C$, was nearly constant at 1.5 cm, independent of the bubble volume in this bubble volume range. The dimension of the bubble C perpendicular to the movement increases with the volume and its depth is considered constant at 1 cm. The volume of the bubble C is given by

$$V_C^* = \frac{l_C^2 L_C}{2}\left[\pi - \frac{(\theta - \sin\theta)}{2}\right] \tag{14}$$

where $l_C$ = 1.5 cm and $\theta$ = 2.46 rad is defined in Figure 3 below. Henceforth, the bubble shape C is called *truncated cylinder*. As the bubble volume increases, the length of the bubble in the direction of the movement also increases and the well-known shape of Fortin [13] is obtained. The depth of the front part reaches 1 cm while the depth of the rear part stays at 0.5 cm. The geometrical ratio $r = b/d_D$ is defined in Figure 4. Three different values of the ratio $r$ have been used in the calculations such as 1/4, 1/3 and 1/2. The volume of the bubble with shape D is given by

$$V_D^* = \frac{d_D^2 h_D}{8}\left[\pi + \cos^{-1}(1-2r) - \frac{1}{2}\sin\left(2\cos^{-1}(1-2r)\right)\right] \tag{15}$$

where $h_D$ = 1 cm.

In the following, the influence of the bubble shape on the electrical resistance is presented for all the shapes introduced in the Figure 2. The bubble volumes are divided in two groups: the intermediate bubbles with a volume less than 20 $cm^3$ and the larger ones called macro-bubbles with a volume ranging from 20 to 80 $cm^3$. The former class includes the *rounded disc* and the *truncated cylinder* shapes while the latter class includes only the Fortin shape. All the results are presented in a relative form using the *circular disc* (shape A) as reference case. For instance, the difference presented on the $y$-axis of the Figures 5, 6 is defined as

$$\text{difference} = \left[\frac{\left.\frac{R_T}{R_0}\right|_{CD} - \left.\frac{R_T}{R_0}\right|_{SB}}{\left.\frac{R_T}{R_0}\right|_{CD}}\right] * 100 = \left[\frac{R_T|_{CD} - R_T|_{SB}}{R_T|_{CD}}\right] * 100 \tag{16}$$

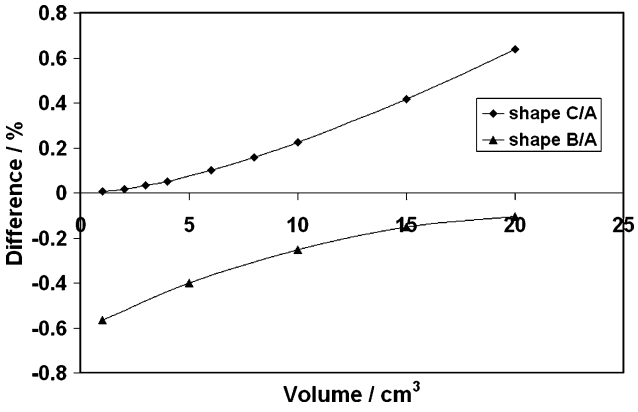


*Fig. 5.* Difference in the electrical resistance for the *rounded disc* (shape B) and the *truncated cylinder* (shape C) bubbles as function of the bubble volume for the intermediate bubble sizes. The base of comparison is the *circular disc* shape (A).

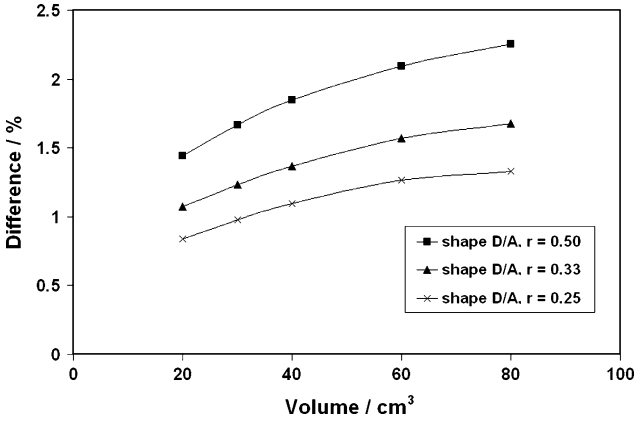


*Fig. 6.* Difference in the electrical resistance for the Fortin shape bubble (shape D) as function of the bubble volume for the macro-bubble sizes. The base of comparison is the *circular disc* shape (A).

where CD is the *Circular Disc* bubble and SB is the *Studied Bubble* shape such as the *rounded disc*, the *truncated cylinder* or the Fortin shape.

Figure 5 shows the influence of the bubble shape on the electrical resistance for the intermediate bubble sizes. The discrepancy between the circular disc bubble and the rounded disc (lower curve) was calculated at a low value of the covering factor to ensure that there is no interaction between the bubble and the limits of the calculation domain. The covering factor is defined as

$$\Theta = \frac{A_p}{A_a} \tag{17}$$

where $A_p$ is the projected bubble area on the anode surface $A_a$. The difference between the *circular disc* bubble and the *truncated cylinder* bubble (upper curve) was computed on an identical surface area of $40 \times 40$ cm$^2$. The difference increases with the bubble volume for the *truncated cylinder* bubble while it decreases for the *rounded disc* bubble. For the former (*truncated cylinder* vs *circular disc*), the increase in difference may not be attributed to the effect of the covering factor since in both cases, it increases proportionally with the bubble volume. The increase of the difference may be explained by the fact that the *circular disc* provokes a stronger, three-dimensional perturbation of the electrical field during the increase of its volume than the *truncated cylinder*. For the latter, the perturbation pattern of the equipotential and current lines stays the same as the increase of the volume is realized by a linear elongation. The difference in the resistance between the *rounded disc* and the *circular disc*(lower curve) is caused mainly by the shape of the bubble extremities. The importance of the edge contribution decreases as the bubble volume increases. Then, the difference decreases as the bubble volume increases. These first results show that for intermediate bubble sizes, the error caused by the use of the *circular disc* shape (A) to simulate the bubbles in a mathematical model that compute the total electrical resistance of the electrolyte is less than 0.7% at low covering factors.

Figure 6 shows the influence of the bubble shape on the electrical resistance for the macro-bubbles, i.e. bubble volumes ranging from 20 to 80 cm$^3$. Once again, the numerical calculations were carried out with a covering factor of 10% based on the *circular disc* bubble to avoid the edge effect. The difference presented on this graph is also defined by Equation 16 but, in this case, the studied bubble is the Fortin shape. First, the values of the resistance difference are one order of magnitude greater than those presented in Figure 5 concerning the intermediate bubble sizes. Second, the influence of the geometrical ratio $r$ on the resistance difference is clear and very interesting. It allows us to compare the contribution of the two phenomena responsible for the increase of the electrical resistance of the electrolyte when a bubble is present: the screening effect and the deformation of the current lines under the bubble. At a given bubble volume, the resistance difference value between the *circular disc* and Fortin shapes is positive and it increases as the ratio increases. These two remarks show the importance of the screening effect compared to the current line perturbation since as the geometrical ratio increases, the covering factor decreases. In other words, the total electrical resistance $R_T$ or the relative resistance $R_T/R_0$ due to the presence of a Fortin shape bubble decreases as the geometrical ratio increases. Furthermore, for the three curves presented in Figure 6, the difference increases slightly with the bubble volume. It is also a very interesting that at the same value of the covering factor the large bubbles provoke a higher electrical resistance than the smaller ones. This remark reflects directly the contribution of the current line deformation to the electrical resistance caused by the presence of the bubble under the anode. In other words, one can say simply that a large bubble deforms the electrical field more than a smaller one even at identical values of the covering factor. The consequence of the latter conclusion may be very important in terms of the influence of the morphological structure of the two-phase layer on the total electrical resistance due to the presence of a large number of bubbles under the anode.

To summarize, the preceding results show that the use of the *circular disc* or the *rounded disc* bubble instead of the Fortin bubble in a mathematical model overestimates the total electrical resistance by less than 2% for the macro-bubble sizes at low covering factors.

The last paragraphs were useful to understand the role of the two contributions to the increment of the electrical resistance when a bubble is present under the anode: the screening effect and the deformation of the current lines under the bubble. But one question still remains: what is the best geometrical configuration to compute the effect of bubble shape on the electrical resistance: the situation where the volume of gas is conserved or when the value of the covering factor is constant ? We must keep in mind that for a bubble-free electrolyte, the current lines are vertical (with the assumptions made earlier). The presence of a bubble deforms the electrical field and a horizontal component of the electrical field is created close to the bubble. Far away from the bubble, the electrical field is homogeneous and the current lines are all vertical. In order to characterize the size of the domain influenced by a bubble, a perturbed region (electrical current tube) of cross-section $A^*$, can be associated which each bubble. The shape of the cross-section of this tube is circular in the case of the bubble shapes A, B, and D and rectangular for the shape C. In this study, the limits of the perturbed zone were defined where the horizontal component of the current density equals 2% of its nominal value, using the results of the numerical solutions. For the evaluation of the effect of the bubble shape, the increment of the electrical resistance caused by a gas volume with a specific shape (A–D) inside its current tube is proposed. The cross-section of the

electrical current tube $A^*$ depends on the volume as well as the shape of the gas pocket. Figure 7 shows the variation of the covering factor $\Theta^*$ for the current tubes with cross-section $A^*$ as function of the bubble volume for the different shapes studied in this work. For the Fortin shape, only the value of $r = 0.25$ is used since it is the most realistic. Indeed, the two other values of $r$ would imply that there is a variation of the pressure within the bubble. It can be seen from Figure 7, that the value of the covering factor within an electrical current tube reaches values higher than 50%. The difference in the relative electric resistances (Equation 16) for the different bubble shapes compared to the *circular disc* (as reference) as function of the bubble volume is presented in Figure 8. The tendency of the curves is the same than the previous ones (computed at low covering factor) with values of the relative difference slightly higher. If the results concerning the Fortin shape are extrapolated, the difference may reach 5% at very high bubble volumes ($V \sim 200$ cm$^3$). According to the interpretation of Richards et al. [18] of direct measurements on industrial cells, the latter values of bubble volumes are only reached under new anodes. With this approach of the characterization of the perturbed zone, the previous conclusions concerning the effect of bubble shape on the electrical resistance are still valid.

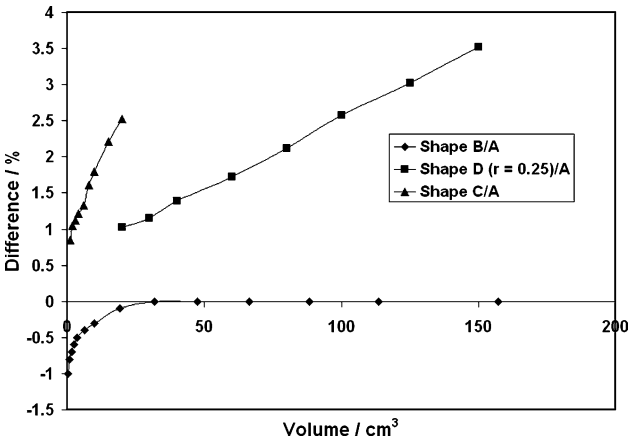


*Fig. 8.* Difference in the relative resistance as function of the bubble volume for the shapes studied in the present work.

### 3.2. *The influence of the wetting film*

In this section, the effect of the thickness of the wetting film on the relative electrical resistance is calculated. It was mentioned above that there exist different regimes of movement for a bubble initially attached under a solid surface. When the equilibrium between the controlling forces is broken for a creeping bubble, the formation of a wetting film begins. At the end of this transition process, the velocity of the bubble is one order of magnitude higher than that in the preceding regime, about 15 cm/s in an air–water gravity driven system. In this regime, the gas is not in contact with the solid surface anymore. There is a liquid film between the bubble and the solid surface. The determination of the thickness of the wetting film is complicated because of the proximity of two interfaces. Presently, the thickness of the wetting film has been estimated to be less than 1.5 mm. Several calculations have been carried out with different bubble shapes and volumes. Figure 9 shows results obtained for the *circular disc* shape for three different volumes. Calculations were done with a covering factor of 30%. Here, the difference presented on the $y$-axis of the graph is defined the same way as earlier by the Equation 16. However in the present case, the reference or the base of comparison is taken for the case when the thickness of the wetting film is zero. This situation corresponds to a bubble in direct contact with the solid surface. The graph shows that the effect of the wetting film on the relative electrical resistance is almost independent of the bubble volume and the difference increases linearly with the thickness of the wetting film. The results presented in Figure 9 are representative of all the calculations performed. Therefore it can be concluded that the influence of the wetting film is less than 2% on the total electrical resistance.

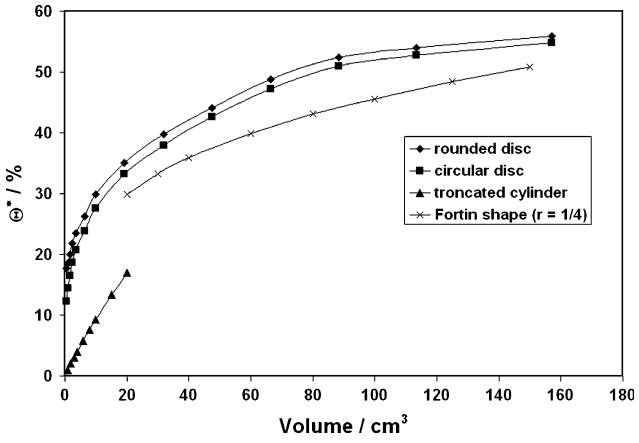


*Fig. 7.* Covering factor in terms of $A^*$, the cross-section of the perturbed zone (electrical current tube), as function of the volume for the different bubble shapes studied in the present work.

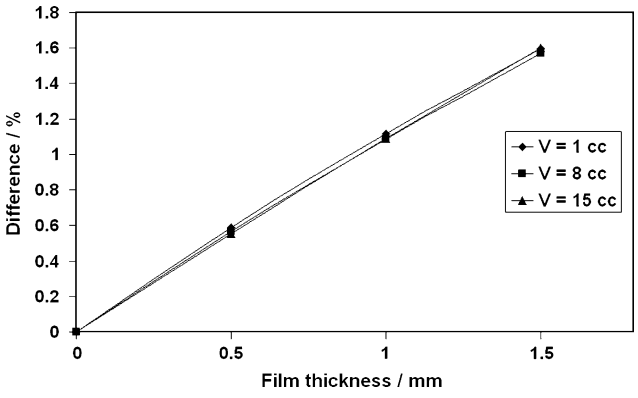


*Fig. 9.* Difference in the electrical resistance as function of the wetting film thickness for three different bubble volumes. The base of comparison is when the thickness of the wetting film is zero.

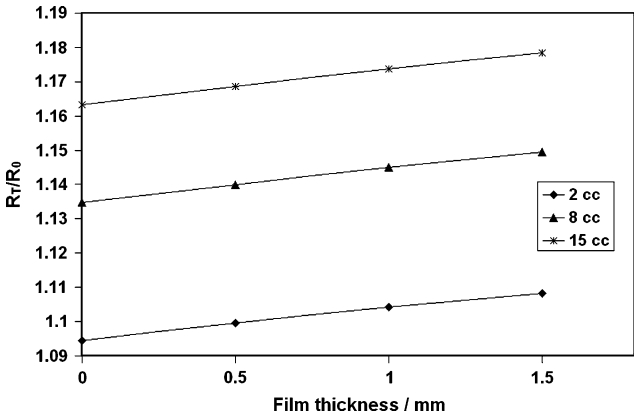


*Fig. 10.* Increase of the relative electrical resistance due to the presence of the wetting film.

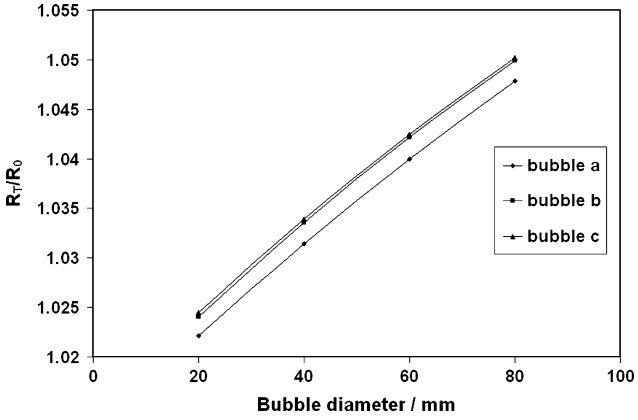


*Fig. 12.* Relative electrical resistance for the configurations shown in Figure 11.

An interesting result presented in Figure 10 is that the relative resistance increases slightly with the thickness of the wetting film. The results for three different bubble volumes are presented such as 2, 8 and 15 $cm^3$. The bubble shape is the circular disc and the covering factor is fixed at 35%. To understand this phenomenon, several tests were carried out with cylindrical bubbles of four different diameters. The geometry is presented in Figure 11. The bubble *a* is attached under the surface with a thickness of 5 mm. In the second situation *b*, the same bubble glides on a wetting film of a thickness of 1 mm. The third bubble *c* is also attached under the surface but its thickness is 6 mm. The anode–cathode distance ACD is kept constant at 5 cm in the three situations. The relative electrical resistance computed for these three situations is presented in Figure 12 below. The results show that the additional resistance caused by the presence of the bubbles *b* and *c* is almost the same. Therefore the increase of the electrical resistance as the wetting film is increased is principally due to a deeper penetration of the deformed zone in the current distribution. Thus the contribution of the small increment of the conducting surface caused by the presence of the wetting film (situation b) is negligible compared to the deflection of the electrical field underneath the bubble.

## 4. Conclusions

In this paper, the influence of the bubble shape on the electrical resistance due to the presence of a single bubble under the anode has been computed by mathematical modeling. Four different shapes have been studied. Three of these shapes have been reported or observed in laboratory. The bubble volumes varied from 1 to 150 $cm^3$. The results show that the influence of the bubble shape for the same volume of gas on the total electrical resistance computed within its perturbed zone (electrical current tube) is less than 5%. The present paper confirms the conclusion of Hyde and Welch [5] that the effect of bubble shape is weak. Furthermore the use of different computational domain sizes allowed us to increase the understanding about the two contributions, such as the screening effect and the deformation of the current lines under the bubble, which are responsible of the resistance increase due to the presence of a bubble under the anode. The effect of the wetting film on the electrical resistance has also been investigated. The thickness of the wetting film varied from 0 to 1.5 mm. The influence of the wetting film has been found negligible with a maximal value of only 2%.

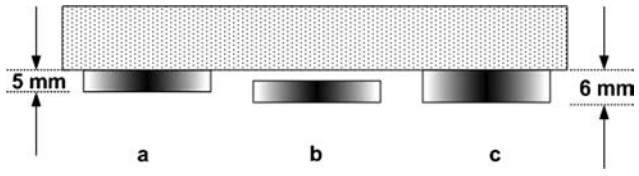


*Fig. 11.* Different bubble geometries.

## Acknowledgements

The first author gratefully acknowledges the support of the Fonds québécois de recherches sur la nature et les technologies (FQRNT) and that of the Conseil de Recherches en Sciences Naturelles et en Génie du Canada (CRSNG) in the form of post-graduate scholarships.

## References

1. K. Grjotheim and H. Kvande (eds.), 'Introduction to Aluminium Electrolysis', 2nd edn. (Aluminium-Verlag, 1993).
2. L.I. Kiss, S. Poncsák, D. Toulouse, A.L. Perron, A. Liedtke and V. Mackowiak, *in* L. Nastac and B.Q. Li (eds.), Light Metals Multiphase Phenomena and CFD Modeling and Simulation in Materials Processes (TMS, Warrendale, PA, 2004), pp. 159–167.
3. W.E. Haupin, *J. Metals* **23** (1971) 46.
4. E. Dernedde and E.L. Cambridge. *in* R. Rentsch (ed.), Light Metals, (TMS, Warrendale, PA, 1975), pp. 111–122.
5. T.M. Hyde and B.J. Welch. *in* R. Huglen (ed.), Light Metals, (TMS, Warrendale, PA, 1997), pp. 333–340.
6. R.J. Aaberg, V. Ranum, K. Williamson and B.J. Welch, *in* R. Huglen. (ed.), Light Metals (TMS, Warrendale, PA, 1997), pp. 341–346.

7. A. Solheim and J. Thonstad. *in* R.B. Miller and W.S. Peterson (eds), Light Metals, (TMS, Warrendale, PA, 1986), pp. 397–403.
8. K. Quian, D. Chen and J.J.J. Chen, *J. Appl. Electrochem.* **28** (1998) 1141.
9. J. Zoric and A. Solheim, *J. Appl. Electrochem.* **30** (2000) 787.
10. H. Vogt and H.D. Kleinschrodt, *J. Appl. Electrochem.* **33** (2003) 563.
11. A.L. Perron, L.I. Kiss and S. Poncsák. *in* H. Kvande (ed.), Light Metals, (TMS, Warrendale, PA, 2005), pp. 565–570.
12. A.L. Perron, L.I. Kiss and S. Poncsák, *Int. J. Multiphase Flow* **32** (2006) 606.
13. S. Fortin, M. Gerhardt and A.J. Gesing. *in* J.P. McGeer (ed.), Light Metals, (TMS, Warrendale, PA, 1984), pp. 721–741.
14. A.L. Perron, L.I. Kiss, S. Poncsák, Int. J. Multiphase Flow (2006) (in press).
15. L.I. Kiss and S. Poncsák. *in* W. Schneider (ed.), Light Metals, (TMS, Warrendale, PA, 2002), pp. 217–223.
16. L.I. Kiss, S. Poncsák and J. Antille. *in* H. Kvande (Ed.), Light Metal (TMS, Warrendale, PA, 2005), pp. 559–564.
17. S. Poncsák, L.I. Kiss, D. Toulouse, A.L. Perron and S. Perron. *in* T.J. Galloway (ed.), Light Metals, (TMS, Warrendale, PA, 2006), pp. 457–462.
18. N. Richards, H. Gudbrandsen, S. Rolseth and J. Thonstad. *in* P.N. Crepeau (ed.), Light Metals, (TMS, Warrendale, PA, 2003), pp. 315–322.